TITLE:

A new standalone microwave instrument for measuring the complex permittivity of materials at microwave frequencies.

AUTHORS:

José D. Gutiérrez-Cano, Pedro Plaza-González, Antoni J. Canós, Beatriz García-Baños, José M. Catalá-Civera, Felipe L. Peñaranda-Foix

ABSTRACT

This paper reports the development of a stand-alone and portable instrument designed to measure the complex permittivity of dielectric materials at microwave frequencies. The equipment consists of an in-house single-port vectorial reflectometer and a resonant coaxial bi-reentrant microwave cavity where the material under test is placed inside a Pyrex vial, making the device appropriate for measuring liquids, semi-solids, powders and granular materials. The relation between the dielectric properties of the involved materials and the cavity resonance has been solved by numerical methods based on mode-matching and circuit analysis. In order to increase the measurement range, so that low to high loss materials can be characterized in the same cavity, the effect of the coupling network is de-embedded from the resonance measurements. The performance of the newly devised instrument is evaluated by error/uncertainty analysis and comparative studies with other well-established instruments and methods. Errors lower than 2% in the dielectric constant, and 5% in the loss factor, are found. This simple, portable, affordable and robust device could help non-specialized personnel to accurately measure dielectric properties of materials used in a wide range of microwave applications.

I. INTRODUCTION

Even though the precise dielectric characterization of materials has been studied for many years, it still remains an important yet challenging task. In fact, dielectric materials have attracted a lot of research interest since they

are widely used in communication applications such as substrates in printed circuit boards (PCB) or dielectric resonators in filters and oscillators [1]-[5].

Moreover, there is an increasing demand for dielectric properties measurements regarding different practical applications in fields like biological and chemical industries [6]-[9], agricultural research [10]-[12], or new food technologies [13]-[15]. Indeed, the study of these properties is relevant for these fields in order to ascertain the ability of dielectric materials to be processed under microwave irradiation [16]. Dielectric properties could then provide scientists and industrial engineers with valuable information to properly incorporate materials into their intended application and to investigate new effective and efficient ways to apply heat into materials and reactions.

The extensive variety of techniques to calculate dielectric properties can be categorized into resonant and non-resonant methods. The criteria used to select the appropriate technique for dielectric characterization mainly takes into account the expected losses of the material under test (MUT), the frequency range covered by the measurement, and the material's attributes (format, shape, homogeneity, etc.).

Resonant methods include resonant cavities, open resonators or dielectric resonators [17]. These techniques make use of the shift in resonant frequency and quality factor of a resonant structure to determine the permittivity of materials at a single frequency [18]. This procedure has become the most preferable for measuring low-loss materials [17]. However, resonant methods might also be considered for measurements of medium and high-loss materials, if the feeding network of the cavities is included in the analysis [19].

Related literature has reported several notable implementations of resonant structures. For instance, Janezic & Baker-Jarvis [20] described a cylindrical structure divided in two halves to measure flat shape materials placed in the gap of the two cylindrical parts. Baker-Jarvis & Riddle [21] presented a full-mode model to extract dielectric properties of cylindrical samples placed inside a reentrant cavity. Krupka [22] used a split-post dielectric resonator to measure laminar-shaped low to medium-loss materials. A common feature in all these procedures is that they require a Vector Network Analyzer (VNA) to generate the microwave signal which is launched into the resonators and to analyze the reflected or transmitted signal that travels back with the information of the dielectric properties of the MUT.

However, VNA devices have several disadvantages. On the one hand, most of them are sophisticated equipment designed to be run in laboratories with specialized operators and which are not or barely portable. On the other hand, the cost of commercial network analyzers, which might be acceptable for the telecommunications sector, is often prohibitive for microwave power industrialists. Microwave industrial processes require specifically designed equipment to be used under industrial conditions: these devices should be simple, portable, affordable and robust, while retaining a useful subset of their current functionality. In fact, most industrial applications only need dielectric properties around ISM frequencies.

Recently, some attempts have been made to develop stand-alone devices to simplify dielectric properties measurements. For example, Korpas [23] reported a system which replaced the VNA by a wideband-magnitude logarithmic power detector to measure dielectric properties of laminar materials together with a single post dielectric resonator. Corbellini and Gavioso [24] described the development and performance of a low-cost and simplified VNA instrument for the measurement of resonances in Quasi-spherical microwave cavities. Likewise, SPEAG (Schmid & Partner Engineering AG) [25] developed an open-ended coaxial probe connected to an integrated and simplified vector reflectometer (R60, Copper Mountain Technologies) to determine dielectric properties without the need of an advanced VNA.

In this paper, we present a portable, stand-alone and easy-to-use instrument which is able to perform reliable and accurate measurements of materials' dielectric properties around the ISM frequency of 2.45 GHz. The device is based on a resonant bi-reentrant microwave cavity where the MUT is placed inside a Pyrex vial, making the device appropriate for measuring liquids, semi-solids, powders and granular materials, as well as solids, if properly machined to fit into the container.

An in-house VNA, consisting of a PLL synthesizer and a dual RF/IF gain and phase receiver, is implemented in the instrument to measure the magnitude and phase of the forward and reflected signals in the microwave cavity. The advent of various wireless technologies during the last years made easy available and cost affordable the selection of microwave components at these frequencies.

The materials' dielectric properties are calculated from the resonant frequency and *Q*-factor measurements and from a full-wave mode-matching analysis of the microwave cavity avoiding any previous calibration with reference materials. Both, frequency synthesizer and receiver are connected to a PC, where user-friendly

LabVIEW-based software allows the automatic control of the measurement process to display the dielectric properties of the MUT in a straightforward way.

By means of this device, low, moderate and high loss materials can be accurately measured, thus providing non-specialized personnel with an accessible system to gain knowledge into the dielectric properties of materials to be used in a wide range of microwave applications.

II. Design of the Measurement Cell

II.A. Microwave Cavity

The dielectric measurement cell is designed as a coaxial bi-reentrant cavity with a partially dielectric filled gap, as shown in Fig. l. The cavity has a coaxial center conductor and an endplate, each with a centered hole. A cylindrical Pyrex tube containing the MUT sample is inserted into the cavity through the endplate hole and further into the center conductor which also provides a concentric alignment.

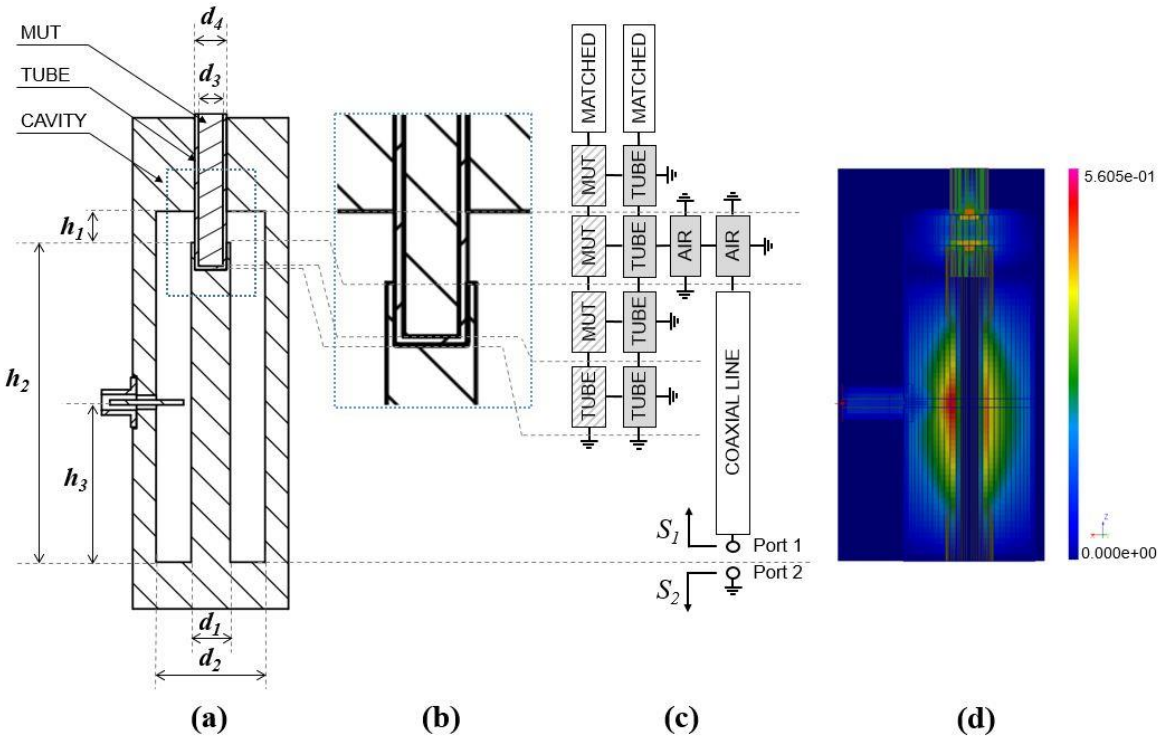

Figure 1. (a) Geometry of the coaxial bi-reentrant microwave cavity, h_1=8mm, h_2=82mm, h_3=41mm, d_1=10mm, d_2=28mm, d_3=6.4mm and d_4=8.2mm. (b) Zoomed image of dotted section in (a). (c) Circuital representation of the microwave cavity used for mode-matching modeling (d) Representation of the E-field in the resonant cavity containing a Pyrex vial filled with a dielectric material simulated by means of a QuickWave 3D Electromagnetic Simulator.

Due to the small size of holes in the coaxial center conductor and endplate in comparison with the wavelength, the electromagnetic fields vanish at these points and therefore the effect of the rounded ends of the Pyrex tube container can be neglected in the structure's electromagnetic modeling.

The relation between the dielectric properties of the MUT and the cavity resonance has been solved by numerical methods based on mode-matching and circuit analysis. These methods have been employed successfully in the technical literature [26] for the analysis of similar coaxial reentrant cavities. The aim of circuit analysis is to split or segment a complex structure into smaller and simpler canonical circuits. These circuit networks, containing N ports, are analyzed and computed separately to obtain multimodal Generalized Scattering (GSM) or Admittance (GAM) Matrices [27], [28]. Next, all the individual matrices are connected together to establish the original structure and also the resonance condition which provides the unloaded resonant frequency f_u and Q_u factor.

In the particular case of the structure depicted in Fig.1., the bi-reentrant cavity was segmented into 21 simpler networks – see Fig.1(c) − with only 5 different circuits: a 2-port network for the coaxial line [27]; a 3-port network (lined background) for the dielectric rod inside the tube and the central part at the bottom of the tube [27]; a 4-port network ring [28] circuit (solid grey background) for the tube enclosing the dielectric material and the air surrounding the tube; a 1-port network for the matched circuits to represent an infinite geometry; and a 1-port network for the finite conductivity short-circuits. Each port in Fig.1(c) was represented by a solid line in the corresponding networks. An equivalence of the different parts of the cavity together with the circuit networks is also shown in Fig. 1. Figure 2 shows the geometry of the 3-port and 4-port networks considered in the mode-matching analysis.

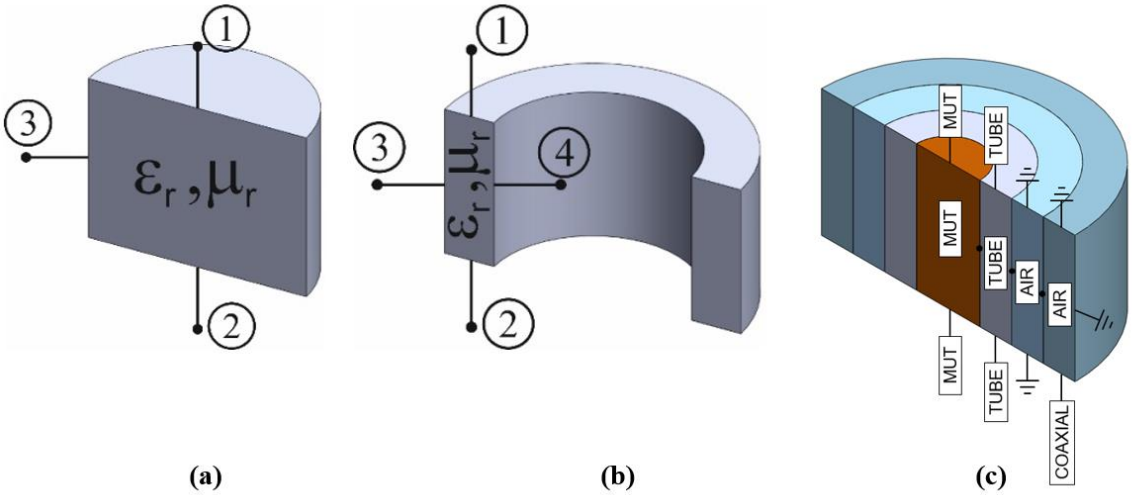

Figure 2. Canonical circuits used for solving the mode-matching and circuit analyses applied to the resonant cavity: (a) 3-port network and (b) 4-port network (c) geometry of the reentrant section of the cavity (h_1 height in Fig.1 (a)) and the network segmentation employed for this zone.

The 3-port structure shown in Fig. 2(a) consists in a dielectric cylinder where port 1 is on the top of the cylinder ($z=h,\ 0<r<a,\ 0<\varphi<2\pi$), port 2 is at the bottom of the cylinder ($z=0,\ 0<r<a,\ 0<\varphi<2\pi$) and port 3 is on the lateral wall ($0<z<h,\ r=b,\ 0<\varphi<2\pi$). This 3-port network can be analyzed by using the GAM matrix [29]-[33] following the procedure described in [20]. Likewise, the 4-port network comprises a ring which is similar to the 3-port network but with an additional inner port at ($0<z<h,\ r=a,\ 0<\varphi<2\pi$), as shown in Fig. 2(b), and the GAM matrix is solved according to [28].

Fig 2(c) shows the geometry of the reentrant section of the cavity (h_1 height in Fig.1(a)) and the network segmentation employed for this zone. The MUT is characterized by a 3-port network connected to the tube in the lateral (port 3 in Fig.2(a)) and to other 3-port MUT sections at the top and bottom (ports 1 and 2 in Fig.2(a)). The region of the tube is characterized by a 4-port network connected in turn to an air section (port 4 in Fig.2(b)) and to other tube networks at the top and bottom. The air sections are also 4-port networks connected to the metal (inner wire) and air coaxial parts.

For each N-port network, the GAM is represented by

$$\vec{\mathbf{e}} = \begin{pmatrix} \vec{e}_1 \\ \vec{e}_2 \\ \dots \\ \vec{e}_N \end{pmatrix} = \begin{pmatrix} \mathbf{Y}_{11} & \mathbf{Y}_{12} & \dots & \mathbf{Y}_{1N} \\ \mathbf{Y}_{21} & \mathbf{Y}_{22} & \dots & \mathbf{Y}_{2N} \\ \dots & \dots & \dots & \dots \\ \mathbf{Y}_{N1} & \mathbf{Y}_{N2} & \dots & \mathbf{Y}_{NN} \end{pmatrix} \cdot \begin{pmatrix} \vec{h}_1 \\ \vec{h}_2 \\ \dots \\ \vec{h}_N \end{pmatrix} = \overline{\overline{\mathbf{Y}}} \cdot \vec{\mathbf{h}} \tag{1}$$

where $\vec{e}_i$ and $\vec{h}_i$ are the coefficients, at port $1 \le i \le N$, of the series expansion of the electric and magnetic field, using appropriate basis functions as described in [27], [28].

Admittance coefficients $\mathbf{Y}_{ij}$ are considered matrices due to the series expansion and the coupling between the ports and the basis functions. Because of the structure's axial symmetry, only the TEM and TM0n modes are expanded in the coaxial and circular waveguides.

The resonant structure is then rebuilt by joining the simpler N-port networks applying the boundary conditions in the common ports (continuity of tangential electric and magnetic fields) as reported in [34]-[36] to calculate the GAM at port 1 (see Fig.1). The relationship between the GAM and the GSM is very simple and has been characterized by [33]. The resonance condition is finally applied to port 1 by means of the following equation [26]

$$\left| S_1(f, \varepsilon_r) \cdot S_2(f) - \mathbf{1} \right| = 0 \tag{2}$$

where $S_1(f,\varepsilon_r)$ refers to the previous GSM calculated at port 1, $S_2(f)$ is the GSM of port 2 (short-circuit at the lower part of the cavity) and *"***1***"* is the symbol of the identity matrix. Eqn. (2) was solved numerically by the Nelder-Mead simplex method [37] which delivered a unique solution within the working frequency range (from 1.9 to 2.6GHz). The solution of the resonant condition of eqn. (2) provides the complex resonant frequency (f_Ω) of the whole original structure according to:

$$f_\Omega = f_u \cdot \left(1 + \frac{j}{2Q_u} \right) \tag{3}$$

The theoretical approach described above was used to determine the dimensions of a resonant measurement cell which provided maximum sensitivity for a wide range of dielectric materials around the frequency of 2.45 GHz (see Fig. 1 for dimensions). Unloaded resonant frequency and *Q*-factor maps, as a function of the dielectric properties obtained by eqn. (2), are displayed in Fig. 3. According to this figure, materials with dielectric

constant ranging from 1 to 100 and losses from 0.001 to 10 will undergo an approximate shift in the resonant frequency from 1.9 to 2.6 GHz (more than 600 MHz) and a *Q*-factor variation from 1,200 to 10.

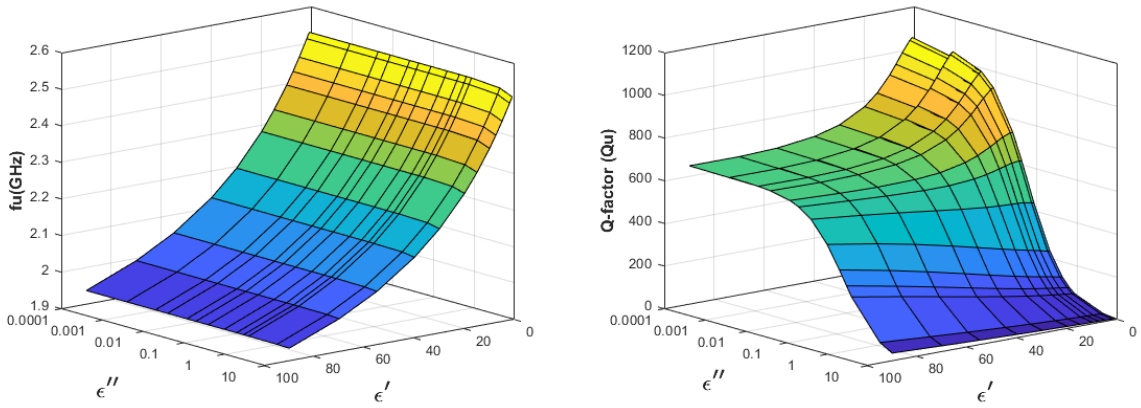

Figure 3. Simulated results (maps) of unloaded resonant frequency (f_u) and *Q*-factor (Q_u) as a function of the dielectric properties ($\varepsilon' - j\varepsilon''$) in the bi-reentrant microwave cavity of Fig. 1

II.B. Coupling Network

The feeding network to couple the energy of the microwave source into the cavity is an electric probe which penetrates some distance into the coaxial cavity, as shown in Fig. 1 (a). Since the coupling mechanism becomes part of the resonant structure, the resonant frequency and *Q*-factor determined from reflection measurements with a VNA (referred as *loaded* and denoted by f_L and Q_L, respectively) shift from the theoretical (*unloaded*) values of the cavity (denoted by f_u and Q_u, respectively).

From a general equivalent circuit, the influence of the coupling on the *Q*-factor has been traditionally modeled in literature by [38]-[41]

$$\frac{1}{Q_L} = \frac{1}{Q_e} + \frac{1}{Q_u} = \frac{k+1}{Q_u} \tag{4}$$

where Q_e stands for the *external* *Q*-factor which accounts for losses in the coupling network and the rest of elements external to the resonator, and $k=Q_u/Q_e$ is the coupling factor. Despite its simplicity and generality,

expression (4) turns out to be very precise and practical since, in addition to Q_L, values of Q_e and k can be also obtained very accurately and directly from the measurement in most cases, and thus the unloaded Q-factor can usually be determined by (4), irrespective of the coupling mechanism used.

However, unlike the Q-factor, the resonant frequency shift due to the coupling cannot be modeled in such a general and precise way, but instead only in terms of parameters directly available from the measured response [19], [40]. The detuning effect of the resonant frequency might be neglected if the energy is weakly coupled into the resonator, in which case unloaded resonant frequencies are practically equal to the loaded resonances ($f_u \approx f_L$). Nonetheless, this undercoupling condition results in an important limitation: medium or high loss materials cannot be measured because they attenuate most of the microwave signal, and the cavity resonance disappears. Consequently, to measure low and high losses in the same cavity, the cavity has to be strongly coupled (overcoupled), and therefore the effect of the coupling network has to be de-embedded from the measurements to retrieve the unloaded resonances.

In this respect, Canós [19] has proposed an empirical technique with which to obtain the unloaded resonant frequency based on reflection measurements of one-port cavities under different coupling levels (i.e. probes of different length), in order to establish a trend towards the uncoupled cavity.

For each coupling condition, values of f_L and Q_e are obtained from applying the Kajfez's linear fractional curve fitting procedure to the measurement of the cavity [40], [42] and the unloaded resonant frequency f_u is estimated through the equation

$$f_L = \left(1 + \frac{A}{Q_e^{\alpha}}\right) \cdot f_u \tag{5}$$

where A and α are fitting parameters related to the electromagnetic fields inside the cavity and the specific coupling network, and remain constant for the different coupling levels.

This technique, which originally involves measurements with variable coupling, has been applied here for de-embedding the cavity's unloaded resonant frequency coupled with a fixed probe, as shown in Fig.1. In this way, the frequency response of six dielectric materials with different permittivity is measured by coupling the cavity with several electrical probes of the same radii and with the same position and orientation as the probe described

in Fig.1, but of different lengths. Pairs of A and α parameters corresponding to the measurement of each material in the cavity for determining the unloaded resonance are represented in Fig. 4 with respect to the loaded resonant frequency f_L of the 10-mm-long probe (Q_e = 119.2).

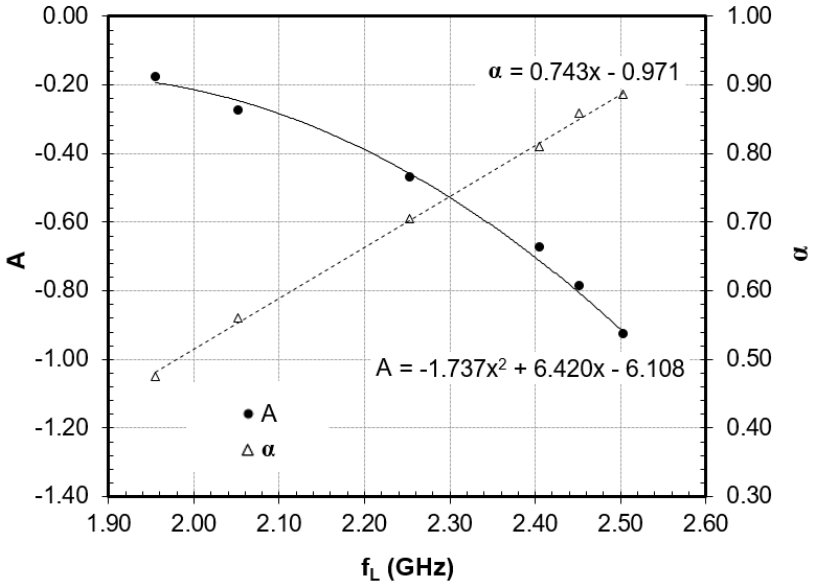

Figure 4. Relationship of A and α with loaded resonant frequency (f_L) for removing the effect of the coupling network.

As Fig. 4 shows, the relationship of A and α with the frequency f_L is very well defined and suitable to be modeled by curve-fitted with simple functions. Through this calibration procedure, A and α can be accurately estimated from the loaded resonant frequency f_L which is measured from the frequency response of the cavity with a fixed probe, and then determine the unloaded resonant frequency f_u by eqn. (5).

The E-field of the bi-reentrant microwave cavity loaded with a dielectric material and coupled with the specific position and length of the coupling probe is modeled using the QuickWave-3D electromagnetic FDTD simulator software (QWED, Warsaw, Poland) and is represented in Fig. 1(b). The figure shows two E-field

variations in the coaxial and bi-reentrant areas corresponding to a resonator length of approximately 3λ/8. The intense E-field in the MUT position is one of the reasons for the high sensitivity of the measurement cell which is reflected in the large frequency shift obtained as a function of the dielectric properties, as illustrated in Fig 3.

III. Experimental set-up

Figure 5 shows a schematic diagram of the in-house portable microwave single-port VNA (PMR) developed for the dielectric measurement of materials. The microwave system consists of four main subsystems: a microwave source, a receiver which detects the magnitude and phases of the forward and reflected microwave signals in order to measure the cavity's reflection (S_{11}), a separation network, and a data acquisition system connected to a personal computer via a USB link.

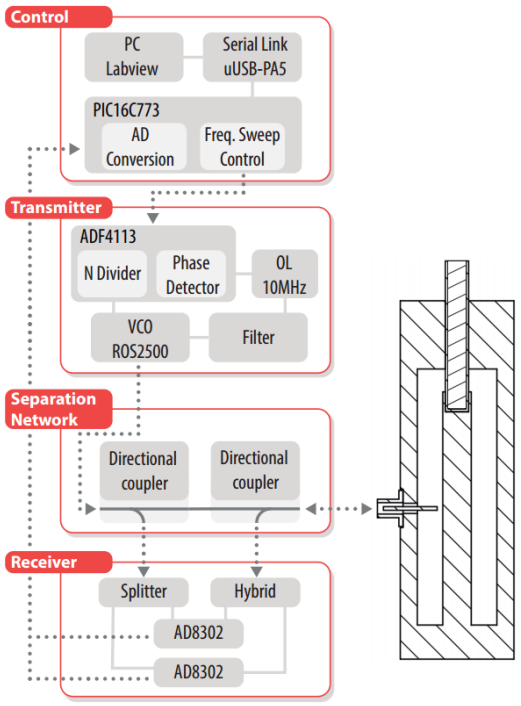

Figure 5. Schematic diagram of the in-house portable microwave single-port VNA (PMR) for measuring the reflection (S_{11}) of the microwave cavity

The transmitter is a PLL frequency synthesizer based on an ADF4113 (Analog Devices) integrated circuit [43]. This chip has a built-in phase detector and an N divider which can implement a complete PLL circuit when used with an external loop filter and a voltage-controlled oscillator (ROS-2500 from Mini-Circuits). This block synthesizes signals that can be rapidly adjusted to generate frequency sweeps from 1,500 to 2,600 MHz, enough to cover the expected range in the resonant cavity measurements.

The receiver was designed from the commercial gain-phase detector AD8302 IC (Analog Devices) [44]. The AD8302 detects the ratio or difference in dBs between two input signals from low frequencies to 2.7 GHz. The circuit integrates two logarithmic detectors on a single chip, each with a dynamic range of 60 dB, a digital phase detector, and circuits used for amplitude and output scaling. The outputs from the AD8302 (V_{MAG} and V_{PHS}) are practically linear voltages from 0 to 1.8 V, proportional to the relative amplitude and relative phase of the two input signals [44]. However, the range for the phase measurement is limited to 0-180 deg. This restriction implies that the AD8302 cannot distinguish between an input phase difference ranging from 0 deg to +180 deg and another ranging from -180 deg and 0 deg. The inherent ambiguity of this circuit was solved here by using two AD8302 devices and adding an extra phase shift (of -90 deg) in one of the units.

Fig.6 illustrates the procedure implemented with the output voltage (V_{PHS}) of the AD8302 circuits in order to solve phase ambiguity. For instance, a V_{PHS} output of 0.68 V in one of AD8302 detectors means that it will not be able to distinguish between the relative phase of points A(-110º) and B(+110º). By shifting the second AD8302 by -90 deg, we can obtain a new V_{PHS} output of 1.6 V where points A and B move to new positions: A'(-20 deg) and B'(20 deg). However, each of these positions again show ambiguity (the phase sign of these positions is unknown again); nonetheless, only points (B-B') result in a phase shift of -90 deg, thus their ambiguity can be solved straightforwardly. Furthermore, the combined outputs of the two AD8302 circuits, once phase ambiguity has been solved, lead to an improvement in the stability of the entire response of the system. For example, the non-linear zones of each AD8302 output (relative phases close to -180 deg, 180 deg or 0 deg, as shown in Fig. 6) were substituted by the linear zone of the alternative AD8302.

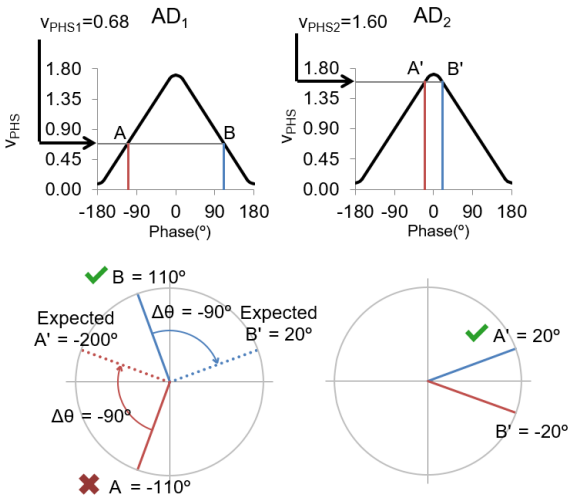

Figure 6. Procedure implemented to solve phase ambiguity in AD8302 IC detectors by shifting two units by -90º

Fig. 5 shows the receiver block system with two AD8302 IC detectors whose input channels are shifted -90 deg by using a 3-dB splitter (S2D1426 from Synergy Microwave Corp) and a 3-dB/-90º hybrid (XC2100A-03 from Anaren). The separation of the forward and reverse signals is carried out by two bi-directional couplers (BDCA 1-7-33+ from Mini-Circuits) to increase directivity.

Output voltage signals from the AD8302 detectors are digitalized in a multichannel 12-bits analog-to-digital converter and processed in a microprocessor (PIC16C773 from Microchip) connected via a serial link to a personal computer. Digital lines for the control of the synthesizer output frequencies are also driven by the microprocessor. A LabVIEW-based software controls all the processes automatically, making the required reflection measurements and transforming the outputs into the desired display (which includes control functionalities, statistics, thresholds, and alarms). This procedure allows several measurement points per second to be obtained. The afore-described setup was assembled in a compact and portable housing. Fig. 7 shows a picture of the developed measurement system.

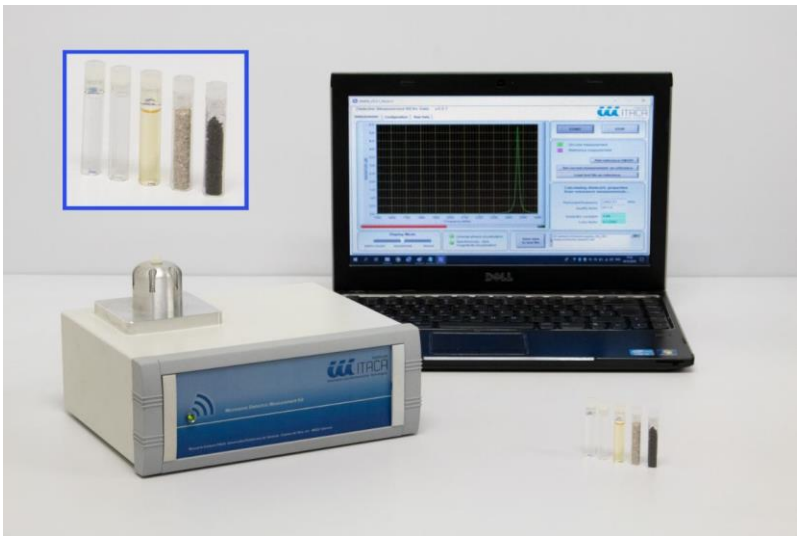

Figure 7. Picture of the Dielectric Measurement Microwave System and zoomed image of the Pyrex vials used to hold the material under test.

IV. Experimental results & Measurements

To evaluate the performance of the in-house dielectric measurement system described in the previous sections, the dielectric properties of eleven well-known reference materials were measured (see Table I). These materials were chosen to cover a broad permittivity and dielectric losses range and then verify the equipment's response under an extensive set of conditions.

In spite of the equipment being designed to characterize solid, powder and liquid materials, we mostly used liquids in these tests to avoid any influence of density or air-gaps of samples in the measurement results. The reference liquids were acquired from Panreac Química (Barcelona, Spain) to ensure the highest reliability of the assays.

In addition, a solid Macor sample from Corning Inc. (NY, USA) machined in the form of a rod of 6.38mm of diameter and a micrometer sized Zeolite powder CBV100 from Zeolyst CV (Farmsum, the Netherlands) with density of 0.51 g/cm3 were included in the dielectric measurements tests.

For all these materials, a detailed error analysis of the permittivity and dielectric loss factor measurements was also performed including uncertainty and a comparative study with other well-established instruments and methods (measurement bias).

IV. A. Resonance Measurements

Fig. 8 shows the magnitude and phase of the S_{11} parameter of the coaxial bi reentrant cavity with Pyrex tubes filled with tetrahydrofuran, acetone and distilled water, measured with the in-house single-port VNA (PMR). These materials were selected because they present dielectric losses which cover both the overcoupled and the undercoupled resonances in the cavity. Measurements of the same cavity and material configuration have also been performed by a commercial full-featured VNA (ZVA50, 2 ports 50GHz, Rohde & Schwarz USA, Inc., Columbia, MD) for comparison purposes. The frequency sweep was set from 1,800 to 2,600 MHz to cover the cavity's frequency range. The IF bandwidth for the VNA measurements was set to 1kHz and both systems used an output power of 0dBm. Prior to measurements, the response of both PMR and VNA were calibrated with the 85052B Standard Mechanical Calibration Kit (3.5 mm, Keysight Technologies, Santa Rosa, CA) and a standard OSM calibration procedure. The S_{11} measurements of the 85052B loads with the full-featured VNA were employed as reference for the calibration of the PMR [45].

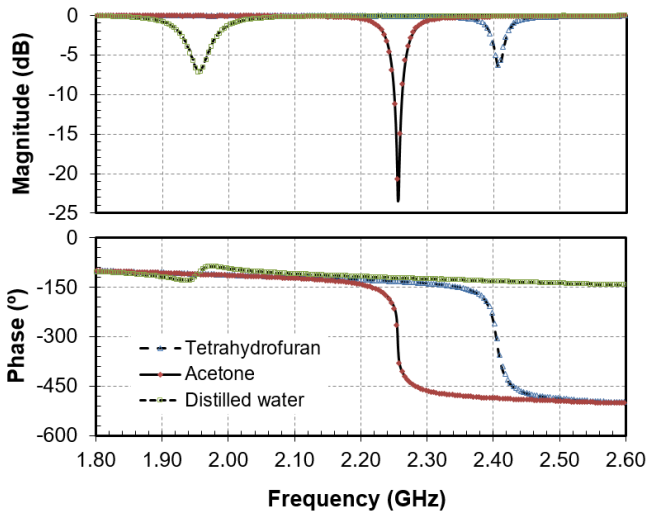

Figure 8. Magnitude and Phase of S_{11} of the coaxial re-entrant cavity with vials filled with tetrahydrofuran, acetone and distilled water measured by an in-house single-port VNA (solid line) and by a commercial full-featured VNA (dashed line)

Results achieved with the in-house VNA (PMR) were in very good agreement with the full-featured VNA since similar resonances overlapped. The magnitude average error was lower than ±0.03 dB and the phase average error was lower than ±0.5 degree.

A series of eight measurements was repeated for each reference liquid in order to assess the type A experimental standard deviation on account of random variations according to [46]. Table I shows the loaded resonant frequencies (f_L) and the unloaded Q-factors (Q_u) determined by S_{11} measurements, according to the procedure described in Section II.

The uncertainties (standard deviations) of the loaded resonant frequencies and Q-factors have the same order of magnitude for both devices, except for those obtained for low-loss materials using the commercial VNA, which showed slightly smaller values. Nevertheless, the resonant frequency uncertainty was constrained below 1 MHz in all cases (even below 200 kHz in the majority), which means a relative resonant frequency uncertainty below 0.05%. The uncertainty of the Q-factor measurements was lower than 0.3% in all cases.

Table I. Complex frequency measurements of the coaxial bi reentrant cavity structure loaded with reference liquids and associated uncertainties. $f_{L\,PMR}$ (MHz), $f_{L\,VNA}$ (MHz) and $|\Delta f_L/f_L|$% are respectively the loaded resonant frequency provided by the PMR and the full featured VNA and their relative difference; $Q_{u\,PMR}$, $Q_{u\,VNA}$, $|\Delta Q_u/Q_u|$% and $|\Delta Q_u|$ are respectively the unloaded Q-factor using the PMR and the full featured VNA and their relative and absolute differences; $f_{u\,rec}$ (MHz), $f_{u\,A\alpha}$ (MHz) and $|\Delta f_u|$ (MHz) are respectively the calculated unloaded resonant frequency and reference and their absolute difference.

MATERIAL	$f_{L\,PMR}$ (MHz)	$f_{L\,VNA}$ (MHz)	$f_{u\,rec}$ (MHz)	$f_{u\,A\alpha}$ (MHz)	$\left\|\frac{\Delta f_L}{f_L}\right\|$%	$\|\Delta f_u\|$(MHz)	$Q_{U\,PMR}$	$Q_{U\,VNA}$	$\left\|\frac{\Delta Q_u}{Q_u}\right\|$%	$\|\Delta Q_u\|$
Empty Tube	2,502.29 ± 0.17	2,502.09 ± 0.06	2,534.58 ± 0.17	2,535.11	0.008	0.525	1,168.8 ± 2.4	1,172.2 ± 1.6	0.290	3.4
Zeolite	2,487.32 ± 0.15	2,487.13 ± 0.06	2,520.82 ± 0.15	2,521.22	0.008	0.398	417.4 ± 1.2	414.6 ± 0.9	0.680	2.8
Cyclohexane	2,485.43 ± 0.12	2,485.28 ± 0.08	2,518.48 ± 0.12	2,518.99	0.006	0.511	1,173.7 ± 1.6	1,177.3 ± 1.0	0.301	3.5
Mineral Oil	2,483.70 ± 0.12	2,483.46 ± 0.03	2,516.83 ± 0.12	2,517.29	0.009	0.458	1,156.4 ± 0.8	1,156.7 ± 0.5	0.028	0.3
Toluene	2,480.10 ± 0.15	2,479.89 ± 0.03	2,513.38 ± 0.15	2,513.79	0.009	0.406	1,016.3 ± 1.4	1,011.7 ± 0.3	0.459	4.6
Oleic Acid	2,480.24 ± 0.23	2,480.05 ± 0.17	2,513.52 ± 0.23	2,514.09	0.008	0.565	664.8 ± 2.0	655.0 ± 1.5	1.499	9.8
2-Propanol	2,451.87 ± 0.06	2,451.02 ± 0.09	2,486.20 ± 0.06	2,484.94	0.034	1.259	27.9 ± 0.0	27.2 ± 0.1	2.536	0.7
Macor	2,430.27 ± 0.16	2,429.88 ± 0.08	2,464.85 ± 0.16	2,465.27	0.016	0.426	834.3 ± 1.7	828.5 ± 0.3	0.702	5.8
Tetrahydrofuran	2,404.34 ± 0.41	2,403.90 ± 0.33	2,440.18 ± 0.40	2,439.11	0.018	1.068	317.3 ± 0.8	310.3 ± 0.9	2.274	7.1
Acetone	2,252.85 ± 0.59	2,252.75 ± 0.45	2,290.68 ± 0.59	2,291.20	0.005	0.522	131.3 ± 0.1	128.6 ± 0.2	2.113	2.7
Dimethyl Sulphoxide	2,051.27 ± 0.18	2,051.70 ± 0.29	2,088.14 ± 0.18	2,090.83	0.021	2.693	15.4 ± 0.0	15.0 ± 0.0	2.880	0.4
Distilled Water	1,955.24 ± 0.94	1,955.02 ± 0.80	1,994.03 ± 0.90	1,991.30	0.011	2.731	44.5 ± 0.1	45.4 ± 0.1	1.983	0.9

Concerning the absolute differences obtained with both systems, the calculated f_L values showed discrepancies of the same order of magnitude as in the uncertainty analysis, i.e. below 0.05%. However, the Q-factor results showed slightly higher discrepancies although constrained below 3% (see the $|\Delta Q_u|$ column in Table I). The influence of these differences on the results of the dielectric properties will be assessed in the following sections.

Unloaded resonant frequencies (f_u) and associated uncertainties (standard deviations) were calculated from the measured f_L of the microwave cavity by means of the regression procedure described in section II.B (see Fig. 4 and eqn. 5) and are also included in Table I. Similar uncertainties to those that were obtained with the unloaded frequencies f_L were measured here.

The unloaded resonant frequencies used as references to analyze absolute deviations (denoted as $f_{u\,A\alpha}$ in Table I) were determined according to [19] with electric probes of different length. The differences found in this comparison between both f_u values ranged from 500 kHz to almost 3 MHz. Thus, the $|\Delta f_u|$ values were used to calculate the uncertainty contribution of the resonant frequency whose results are presented in Section IV.C.

IV. B. Dielectric Measurements

The average unloaded resonant frequencies and Q-factors of Table I were employed to calculate dielectric properties with the numerical procedure described in Section II.A. Results are given in Table II.

Table II. Dielectric properties results of reference liquids and associated uncertainties.

MATERIAL	ε'_{ref}	ε''_{ref}	ε'_{calc}	ε''_{calc}	$\left\|\frac{\Delta\varepsilon'}{\varepsilon'}\right\|\%$	$\left\|\frac{\Delta\varepsilon''}{\varepsilon'}\right\|\%$
Ciclohexane	1.99 ± 0.03	0.0000 ± 0.0000	2.02 ± 0.05	0.0000 ± 0.0003	1.31	-
Zeolite	1.86 ± 0.04	0.1193 ± 0.0060	1.88 ± 0.04	0.1244 ± 0.0018	1.29	4.28
Mineral Oil	2.18 ± 0.03	0.0015 ± 0.0002	2.16 ± 0.04	0.0014 ± 0.0003	0.73	4.83
Toluene	2.43 ± 0.10	0.0109 ± 0.0005	2.42 ± 0.04	0.0112 ± 0.0005	0.25	2.95
Oleic Acid	2.37 ± 0.03	0.0444 ± 0.0010	2.37 ± 0.05	0.0442 ± 0.0019	0.17	0.62
2-Propanol	4.03 ± 0.20	3.1642 ± 0.3100	4.09 ± 0.09	3.2325 ± 0.0810	1.49	2.16
Macor	5.68 ± 0.03	0.0238 ± 0.0006	5.74 ± 0.05	0.0228 ± 0.0009	1.13	4.36
Tetrahydrofuran	7.61 ± 0.31	0.1922 ± 0.0370	7.57 ± 0.10	0.1939 ± 0.0069	0.53	0.92
Acetone	21.44 ± 0.21	0.8652 ± 0.1600	21.21 ± 0.18	0.8239 ± 0.0214	1.08	4.78
Dimethyl Sulphoxide	45.65 ± 0.39	9.3514 ± 1.0100	45.08 ± 0.71	9.5052 ± 0.4013	1.26	1.64
Distilled Water	78.47 ± 1.08	6.8709 ± 1.2200	77.51 ± 1.07	6.9014 ± 0.1691	1.22	0.45

The dielectric properties of all MUTs were also measured at similar frequencies through other well-established techniques from the literature to obtain a set of values to be used as reference data for estimating the accuracy of the developed method (measurement bias). We selected the techniques to achieve the most reliable results depending on the losses of each liquid. Thus, liquid MUTs with higher losses were measured with an open-ended coaxial resonator [47], whereas liquid MUTs with lower losses were measured with a fully-loaded cylindrical cavity [48]. Macor was measured with a partially filled cylindrical cavity [14], [28] and the Zeolite powder by the dual mode cylindrical cavity of [14]. The percentage given in Table II was calculated as the relative difference (bias) between the calculated dielectric properties and the reference values.

The dielectric properties measured with the proposed method agreed well with the reference values. Therefore, the estimated accuracy obtained for the dielectric constant was within the range of 1.5% in all the covered measurements, regardless of the material losses. The error in the loss factor was constrained around 5% in the considered measurement range. These results regarding the accuracy of the losses are particularly relevant since the losses of the materials spread throughout 4 orders of magnitude (from 10^{-3} to 10^{1}).

The developed device provides the dielectric properties of the MUT inside the Pyrex tube as a bulk material. Therefore, it is important to remark that for powder or particulate materials, density and even moisture fluctuations in the sample can cause significant deviations in the dielectric measurements. To overcome this

situation, numerous density and moisture independent calibration algorithms have been successfully tested in the technical literature from the dielectric properties of particulate materials at different air-particle mixture ratio [49]. For solid materials, it has been empirically tested that samples must be precisely machined in the form of rods with an air gap between the solid sample and the Pyrex tube no larger than 0.01mm in order to keep an equivalent accuracy to the liquid samples.

Although accuracy was fairly stable across the studied materials, the measurement range was limited by the MUT losses, when the *Q*-factors dropped below 15, as the interpolation for the calculation of *Q* proved difficult to obtain reliable values.

IV.C. Uncertainty of Permittivity Measurements

Even though a comparative review through other well-established instruments and methods was undertaken, the accuracy of the proposed technique depends on the uncertainties of the different magnitudes involved in the numerical procedure given by eqns. (1) and (2). These uncertainties include those of the unloaded resonances derived from the measurements using the in-house single-port VNA as well as the dimensional errors arising from the manufacturing tolerances of the resonant structure and the tubes used as holders (e.g. differences between the real dimensions of the resonant fixture and the values assumed in the computations).

The effect of these errors on the uncertainty of the computed permittivity values has been calculated taking into account the law of uncertainty propagation, or combined standard uncertainty, as carried out by GUM [46]. This effect is described in [27] for permittivity measurements and reproduced below. Assuming uncorrelated variables, the permittivity uncertainty can be computed as:

$$\partial\varepsilon_{r1} = k_p \cdot \sqrt{\sum_i \left(\frac{\partial\varepsilon_{r1}}{\partial x_i} \cdot \Delta x_i \right)^2} \tag{6}$$

where x_i are the different variables involved in the uncertainty of the measurement, Δx_i is the uncertainty associated with each variable, and $\partial\varepsilon_{r1}/\partial x_i$ are the partial derivatives of the permittivity depending on the

variable used and k_p is the coverage factor. In this work k_p was fixed to 1 assuming a normal distribution with a level of confidence of 68.27%.

The uncertainties of the unloaded resonant frequency and *Q*-factor described in this section are given in Table I (denoted as $|\Delta f_u|$ and $|\Delta Q_u|$). With regard to the manufacturing tolerances, the inspection of the cavity parts showed the following dimensional uncertainties: the cavity's radius was ±20 μm; the radius of the inner coax wire, ±10 μm; the height of the coaxial part, ±10 μm; the height of the cylindrical part, ±10 μm; the internal radius of the Pyrex tube, ±10 μm; and the external radius of the Pyrex tube was ±10 μm.

Derivatives of eqn. (6) were calculated through numerical methods, due to the difficulty of finding an analytical expression, as shown in [27]. The uncertainties calculated with this procedure are presented in Table II together with the average values.

For all considered liquids, the uncertainty was within the range of 2% for the dielectric constant and 5% for the loss factor. The uncertainties obtained for the low-loss materials were very close to those obtained with reference cavity methods, which is remarkable bearing in mind the usage of a fixed coupling network.

Table III. Uncertainty contributions of the involved parameters to the total uncertainty calculation for acetone (refer to Fig.1 and Table I to ascertain the definition of the parameters).

x_i	Δx_i	$\frac{\partial \varepsilon'}{\partial x_i}\cdot\Delta x_i$	$\frac{\partial \varepsilon''}{\partial x_i}\cdot\Delta x_i$
d_1	20μm	0.03	0.0010
d_2	40μm	0.03	0.0012
d_3	20μm	0.15	0.0154
d_4	20μm	0.03	0.0026
h_1	10μm	0.01	0.0000
h_2	10μm	0.02	0.0004
$\|\Delta f_u\|$	0.522MHz	0.07	0.0011
$\|\Delta Q_u\|$	2.7	0.00	0.0145
$\partial \varepsilon_{r1}$		0.18	0.0214

Table III. shows the individual contribution of each variable involved in the uncertainty of the measurements, for a representative material as acetone. The manufacturing tolerances of the Pyrex tubes often caused the highest influence in the total uncertainty for both, dielectric constant and loss factor. Uncertainties of the resonant frequency and Q-factor measurements $|\Delta f_u|$ and $|\Delta Q_u|$ also exhibited important contributions to the total uncertainty. The influence of the rest of parameters was limited, as indicated in the Table.

V. CONCLUSIONS

In this paper, a compact, robust, portable and standalone microwave system to measure the permittivity of dielectric materials around the ISM band 2,45 GHz has been described.

The measurement process consisted in placing a Pyrex vial containing a sample of material inside a bi-reentrant microwave cavity and measuring the resonant parameters of the cavity with an in-house portable microwave reflectometer. A LabVIEW-based software controlled all the processes automatically, making the measurement process very simple and straightforward. The device especially appropriate for measuring liquids, semi-solids, powders and granular materials can also be used for solids, if properly machined to fit into the container.

The microwave cavity has been analyzed using numerical methods based on mode-matching and circuit analysis. Unlike previous efforts to design dielectric properties measurement methods, the system described in this paper allowed the characterization of both high and low loss dielectric materials by means of a procedure that removes the effect of the coupling network from the complex resonance.

A detailed error analysis of the permittivity and dielectric loss factor measurements was also performed including uncertainty and a comparative study with other well-established instruments and methods. The estimated accuracy obtained for the dielectric constant was within the range of 1.5% and the error in the loss factor was constrained around 5% in the considered measurement range. These results regarding the accuracy of the losses are particularly relevant since the losses of the materials spread throughout 4 orders of magnitude (from 10^{-3} to 10^{1}).

The developed system is a very promising device to obtain dielectric properties measurements in a wide range of industrial microwave applications.

VI. ACKNOWLEDGMENT

This paper has been financially supported through the grant reference BES-2016-077296 of the call Convocatoria de las ayudas para contratos predoctorales para la formación de doctores de 2016 by Ministerio de Economía y Competitividad (MINECO) and by European Social Funds (ESF) of European Union and the project SEDMICRON - TEC2015-70272-R (MINECO/FEDER) supported by Ministerio de Economía y Competitividad (MINECO) and by European Regional Development Funds (ERDF) of European Union.

VII. REFERENCES

[1] Z. Wang, J. Liu and L. Liu, "Permittivity measurement of $Ba_{0.5}Sr_{0.5}TiO_3$ ferroelectric thin films on multilayered silicon substrates," *IEEE Trans. Instrum. Meas.*, vol. 55, no. 1, pp. 350–356, Feb. 2006.

[2] A. Sahu, P. H. Aaen, A. Lewandowski, M. Shkunov, G. Rigas, P. T. Blanchard, T. M. Wallis, and V. K. Devabhaktuni, "Robust microwave characterization of inkjet-printed coplanar waveguides on flexible substrates," *IEEE Trans. Instrum. Meas.*, vol. 66, no. 12, pp. 3271–3279, Dec. 2017.

[3] J. Krupka, M. E. Tobar, J. G. Hartnett, D. Cros and J. M. Le Floch, "Extremely high-Q factor dielectric resonators for millimeter-wave applications," *IEEE Trans. Microw. Theory Tech*., vol. 53, no. 2, pp. 702-712, Feb. 2005.

[4] M. T. Sebastian, R. Ubic & H. Jantunen, "Low-loss dielectric ceramic materials and their properties," *Int. Mater. Rev.*, vol. 60, no. 7, pp. 392-412, Jul. 2015.

[5] Y. Kato and M. Horibe, "New permittivity measurement methods using resonant phenomena for high-permittivity materials," *IEEE Trans. Instrum. Meas.*, vol. 66, no. 6, pp. 1191–1200, Jun. 2017.

[6] B. Mohammed, K. Bialkowski, A. Abbosh, P. C. Mills, and A. P. Bradley, "Dielectric properties of dog brain tissue measured in vitro across the 0.3-3 GHz band," *Bioelectromagn.*, vol. 37, no. 8, pp. 549–556, Sep. 2016.

[7] L. Abdilla, C. Sammut, and L. Z. Mangion, “Dielectric properties of muscle and liver from 500 MHz-40 GHz,” *Electromagn. Biol. Med.*, vol. 32, no. 2, pp. 244–252, Jun. 2013.

[8] P. Mehta, K. Chand, D. Narayanswamy, D. G. Beetner, R. Zoughi and W. V. Stoecker, "Microwave reflectometry as a novel diagnostic tool for detection of skin cancers," *IEEE Trans. Instrum. Meas.*, vol. 55, no. 4, pp. 1309-1316, Aug. 2006.

[9] Y. Gao, M. T. Ghasr, M. Nacy and R. Zoughi, “Towards Accurate and Wideband In Vivo Measurement of Skin Dielectric Properties,” *IEEE Trans. Instrum. Meas.*, vol. 68, no. 2, pp. 512-524, Feb. 2019.

[10] S. O. Nelson, *Dielectric Properties of Agricultural Materials and Their Applications*. New York, NY, USA: Elsevier - Academic Press, 2015.

[11] B. L. Shrestha, H. C. Wood and S. Sokhansanj, "Microwave Dielectric Properties of Alfalfa Leaves From 0.3 to 18 GHz," *IEEE Trans. Instrum. Meas.*, vol. 60, no. 8, pp. 2926-2933, Aug. 2011.

[12] Y. L. Then, K. Y. You, M. N. Dimon and C. Y. Lee, “A modified microstrip ring resonator sensor with lumped element modeling for soil moisture and dielectric predictions measurement,” Measurement, vol. 94, pp. 119-125, Dec. 2016.

[13] M. S. Venkatesh and G. S. V. Raghavan, “An Overview of Microwave Processing and Dielectric Properties of Agri-Food Materials,” Biosyst. Eng., vol. 88, no. 1, pp. 1-18, May 2004.

[14] J. D. Gutiérrez, J. M. Catalá-Civera, J. Bows and F. L. Peñaranda-Foix, “Dynamic measurement of dielectric properties of food snack pellets during microwave expansion,” *J. Food Eng.*, vol. 202, pp. 1-8, Jun. 2017.

[15] M. Naderi-Boldaji, P. Mishra, M. Ahmadpour-Samani, M. Ghasemi-Varnamkhasti, D. Ghanbarian and Z. Izadi, “Potential of two dielectric spectroscopy techniques and chemometric analyses for detection of adulteration in grape syrup,” *Measurement*, vol. 127, pp. 518-524, Oct. 2018.

[16] D.A. Jones, T.P. Lelyveld, S.D. Mavrofidis, S.W. Kingman and N.J. Miles, “Microwave heating applications in environmental engineering—a review,” *Resour. Conserv. Recycl.*, vol. 34, no. 2, pp. 75-90, Jan. 2002.

[17] J. Krupka, “Frequency domain complex permittivity measurements at microwave frequencies,” *Meas. Sci. Technol.*, vol. 17, pp. R55–R70, Sep. 2005.

[18] J. Baker-Jarvis, M. D. Janezic and D. C. Degroot, "High-frequency dielectric measurements," *IEEE Instrum. Meas. Mag.*, vol. 13, no. 2, pp. 24-31, Apr. 2010.

[19] A. J. Canós, J. M. Catalá-Civera, F. L. Peñaranda-Foix, and E. Reyes-Davó, “A novel technique for deembedding the unloaded resonance frequency from measurements of microwave cavities,” *IEEE Trans. Microw. Theory Techn.*, vol. 54, no. 8, pp. 3407–3416, Aug. 2006.

[20] M. D. Janezic and J. Baker-Jarvis, “Full-wave analysis of a split-cylinder resonator for nondestructive permittivity measurements,” *IEEE Trans. Microw. Theory Tech.*, vol. 47, no. 10, pp. 2014-2020, Oct. 1999.

[21] J. Baker-Jarvis and B. F. Riddle, “Dielectric Measurements Using a Reentrant Cavity: Mode-Matching Analysis”. *NIST Tech. Note 1384*, Nov. 1996.

[22] J. Krupka, R. N. Clarke, O. C. Rochard, and A. P. Gregory, “Split post dielectric resonator technique for precise measurements of laminar dielectric specimens—Measurement uncertainties,” in *Proc. 13th Int. Conf. Microw., Radar & Wireless Commun.*, Wroclaw, Poland, May 22–24, 2000, pp. 305–308.

[23] P. Korpas, W. Wojtasiak, J. Krupka and W. Gwarek, "Inexpensive approach to dielectric measurements," *in 19th Int. Conf. Microw., Radar & Wireless Commun.*, Warsaw, May 22–24, 2012, pp. 154-157.

[24] S. Corbellini and R. M. Gavioso, "A Low-Cost Instrument for the Accurate Measurement of Resonances in Microwave Cavities," *IEEE Trans. Instrum. Meas.*, vol. 62, no. 5, pp. 1259-1266, May 2013.

[25] SPEAG, Schmid & Partner Engineering AG, Zurich, Switzerland. *DAK - Dielectric Assessment Kit Product Line*. [Online]. Available: http://www.speag.com/products/dak/dielectric-measurements, Accessed on: Oct. 24, 2018.

[26] F. L. Peñaranda-Foix, J. M. Catala-Civera, A. J. Canos-Marin and B. Garcia-Baños, “Circuital analysis of a coaxial re-entrant cavity for performing dielectric measurement”, in *2009 IEEE MTT-S Int. Microw. Symp. Dig.*, Boston, MA, USA, Jun. 7-12, 2009, pp. 1309–1312.

[27] F. Penaranda-Foix and J. M. Catalá-Civera, “Circuital analysis of cylindrical structures applied to the electromagnetic resolution of resonant cavities,” in *Passive Microwave Components and Antennas*, V. Zhurbenko, Ed. Rijeka, Croatia: In-Tech, 2010, ch. 7, pp. 141–168.

[28] F. L. Penaranda-Foix, M. D. Janezic, J. M. Catala-Civera, and A. J. Canos, “Full-wave analysis of dielectric-loaded cylindrical waveguides and cavities using a new four-port ring network,” IEEE Trans. Microw. Theory Techn., vol. 60, no. 9, pp. 2730–2740, Sep. 2012.

[29] J. Rubio, M. A. Gonzalez and J. Zapata, "Rigorous mutual coupling analysis of open-ended radiating structures based on SFELP(segmentation technique/finite elements/Lanczos-Pade) and spherical modes," in *IEEE Antenna Propagat. Soc. Int. Symp.*, Columbus, OH, USA, Jun. 22-27, 2003, vol. 2, pp. 197-200.

[30] J. M. Rebollar, J. Esteban and J. E. Page, "Fullwave analysis of three and four-port rectangular waveguide junctions," *IEEE Trans. Microw. Theory Techn.*, vol. 42, no. 2, pp. 256-263, Feb. 1994.

[31] F. Alessandri, M. Mongiardo, and R. Sorrentino, “Rigorous mode analysis of mitered E-plane bends in rectangular waveguides*,” IEEE Trans. Microw. Guided Wave Lett.*, vol. 4, no. 12, pp. 408–410, Dec. 1994.

[32] H. Auda and R. F. Harrington, "A Moment Solution for Waveguide Junction Problems," *IEEE Trans. Microw. Theory Techn.*, vol. MTT-31, no. 7, pp. 515-520, Jul. 1983.

[33] G. Conciauro, M. Guglielmi, and R. Sorrentino, *Advanced Modal Analysis-CAD Techniques for Waveguide Components and Filters*. New York, NY, USA: Wiley, 2000.

[34] F. L. Peñaranda-Foix, “Application of the Generalized Circuital Analysis to Solve Electromagnetic Diffraction Problems,” Ph.D. dissertation, Univ. Politècnica de València, Valencia, Spain, 2001.

[35] E. Diaz Caballero, A. Belenguer, H. Esteban and V. E. Boria, "Extending the Cascading by Pairs of Multiport Generalized Scattering Matrices for Characterizing the Connected Ports*," IEEE Microw. Wirel. Compon. Lett.*, vol. 24, no. 11, pp. 733-735, Nov. 2014.

[36] A. Belenguer, E. Diaz Caballero, H. Esteban, A. L. Borja and J. Cascon, "Krylov's Solver Based Technique for the Cascade Connection of Multiple n-Port Multimodal Scattering Matrices," *IEEE Trans. Microw. Theory Techn.*, vol. 61, no. 2, pp. 720-726, Feb. 2013.

[37] J. C. Lagarias, J. A. Reeds, M. H. Wright, and P. E. Wright, “Convergence properties of the Nelder-Mead simplex method in low dimensions,” *SIAM J. Optimiz.*, vol. 9, no. 1, pp. 112–147, 1998.

[38] E. L. Ginzton, *Microwave Measurements*. New York, NY, USA: McGraw-Hill, 1957.

[39] J. E. Aitken, "Swept-frequency microwave Q-factor measurement," *Proc. Inst. Elec. Eng.*, vol. 123, no. 9, pp. 855-861, Sep. 1976.

[40] D. Kajfez, *Q Factor*. Oxford, MS: Vector Fields Ltd., 1994.

[41] A. Luiten, “Q-Factor Measurement,” in *Wiley Encyclopedia of Electrical and Electronics Engineering*, New York, NY, USA: Wiley, 1999. pp. 477-491.

[42] D. Kajfez, “Linear fractional curve fitting for measurement of high Q-factors,” *IEEE Trans. Microw. Theory Tech.*, vol. 42, no. 7, pp. 1149–1153, Jul. 1994.

[43] Analog Devices, Inc. *RF PLL Frequency Synthesizers ADF4116/ ADF4117/ ADF4118*. [Online]. Available: https://www.analog.com/media/en/technical-documentation/data-sheets/ADF4116_4117_4118.pdf, Accessed on: Feb. 12, 2018.

[44] Analog Devices, Inc. *RF/IF Gain and Phase Detector AD8302*. [Online]. Available: https://www.analog.com/media/cn/technical-documentation/evaluation-documentation/ AD8302.pdf, Accessed on: Feb. 12, 2018.

[45] M. Hiebel, “Vector network analyzer (vna) calibration: The basics,” *Rohde & Schwarz, Tech. Rep.*, 2008.

[46] Bureau International des Poids et Mesures (BIPM), *Evaluation of Measurement Data-Guide to the Expression of Uncertainty in Measurement, JCGM 100:2008*. [Online]. Available: https://www.bipm.org/ utils/common/documents/jcgm/JCGM_100_2008_E.pdf, Accessed on: Dec. 3, 2018.

[47] A. J. Canós Marín, B. García-Baños, J. M. Catalá-Civera, F. L. Peñaranda-Foix and J. D. Gutiérrez-Cano, "Improvement in the Accuracy of Dielectric Measurement of Open-Ended Coaxial Resonators by an Enhanced De-Embedding of the Coupling Network," *IEEE Trans. Microw. Theory Techn.*, vol. 61, no. 12, pp. 4636-4645, Dec. 2013.

[48] R. E. Collin, *Foundations for Microwave Engineering*, 2nd ed. New York, NY, USA: McGraw-Hill, 1992

[49] S. Trabelsi, A. M. Paz and S. O. Nelson, “Microwave dielectric method for the rapid, non-destructive determination of bulk density and moisture content of peanut hull pellets”, *Biosyst. Eng.*, vol. 115, no. 3, pp. 332–338, Jul. 2013.